

RESEARCH

Open Access



# Modeling of vertical microplastic transport by rising bubbles

Moritz Lehmann\*, Fabian P. Häußl and Stephan Gekle

## Abstract

Microplastic particle concentration at the sea surface is critical for quantifying microplastic transport across the water-air interface. Previous studies suggest that the concentration at the sea surface is enhanced compared to bulk concentration, yet little is known about the detailed mechanisms behind this enhancement. In this work, we model one particular process in simulation that may contribute to this enhanced surface concentration: bubble scavenging. Using lattice-Boltzmann Volume-of-Fluid simulations, we find that rising bubbles indeed generate a net flow of particles toward the surface. The efficiency of the process, however, highly depends on the microplastic particle surface properties. Clean, hydrophobic particles adhere much better to the bubble surface and are therefore transported significantly better than weathered, hydrophilic particles that are only entrained in the flow around a bubble.

**Keywords** Microplastics, Bubbles, Sea surface, Lattice Boltzmann method, Volume-of-Fluid, GPU, OpenCL

## Introduction

Waves on the ocean surface create myriads of air bubbles [1] that rise to the surface and burst. During rise, bubbles can interact with particles suspended in the water [2–7] and enrich particle concentration prior to bubble burst by bubble scavenging [8–12]. At burst, bubbles eject fine water droplets into the air, either in the form of film droplets or jet droplets of various size depending on bubble diameter [13–21]. This process is associated with aerosol production [10, 22–25], including bacteria [26, 27] and organic compounds [28]. Besides these, bursting can also lead to the ejection of microplastic particles into the air [29–33] similar to microplastic ejection by impacting raindrops [34].

Knowing the concentration of microplastic particles in the sea surface microlayer (SML) is key for estimating environmental relevance of this water-air transport. Experimental studies show large local variations in

marine microplastic particle concentration [35–38], and find that concentration at the SML is largely enhanced compared to bulk concentration [39–41], yet don't identify the mechanisms leading to this difference in concentration between SML and bulk.

In this work we investigate vertical microplastic transport in the water column with the bubble scavenging mechanism by using computer simulations. Specifically we aim to understand the impact of particle wetting properties on transport efficiency.

## Methods

### Volume-of-Fluid lattice Boltzmann method

In this work we use the Volume-of-Fluid (VoF) lattice Boltzmann method (LBM) implementation *FluidX3D* [34, 42–47] that has been extended to simulate rising bubbles with Hoshen-Kopelman [48] volume tracking and the ideal gas law

$$pV = nRT = \text{const.} \quad (1)$$

The method is thoroughly validated in [34, 44–47, 49]. VoF provides three classes of Cartesian grid points – fluid, interface and gas. The fluid phase is simulated with regular LBM, the interphase is kept sharp at a thickness

\*Correspondence:

Moritz Lehmann  
moritz.lehmann@uni-bayreuth.de  
Biofluid Simulation and Modeling – Theoretische Physik VI, University of Bayreuth, Bayreuth, Germany

of one lattice cell and handles surface tension, and the gas phase is not simulated and treated as vacuum. To accommodate for bubbles, all separate gas domains are tracked with a Hoshen-Kopelman approach, computing their volume and pressure. Since our simulations are isothermal, the product  $pV$  must remain constant, which is ensured by modifying density in reconstructed gas equilibrium populations in the VoF-LBM model. Special consideration is given to events when a bubble splits in two or more smaller bubbles or when two or more bubbles merge, for which trigger events are detected [47].

### Immersed-boundary method

Microplastic particles are modeled by the immersed-boundary method (IBM) as in [34, 42]. A single IBM point-particle (with an effective hydrodynamic diameter of the lattice constant) corresponds to one microplastic particle. These IBM particles are neutrally buoyant and do not interact with each other, reflecting the natural situation where the microplastic concentration is expected to be rather low (between 1 to 7 particles per liter [35, 50]). Neutral buoyancy simplifies the IBM to one-way-coupling, meaning particles are only passively advected by the velocity field and interface forces and do not exert forces back on the fluid. In addition, the non-interaction allows us to simulate high particle concentrations for statistically meaningful results and then linearly scale down concentrations to environmental estimates. Unlike in an experiment, where such a large concentration would significantly increase Einstein viscosity, there is no change in viscosity in the simulation as the particles are modeled as point-particles rather than spheres.

For this study, the interaction of the particles with the water surface is critical. We consider two scenarios:

- 1 Non-sticky particles: Particles are only prevented from leaving the water phase with a repelling hard potential as in [34].
- 2 Sticky particles: Particles are prevented from leaving the water phase with a repelling hard potential as in [34], but additionally, once entering the direct vicinity of the water surface (distance of one lattice cell or less), a second attracting hard potential locks them onto the surface.

A technical difficulty in both situations is that the exact surface position in VoF-LBM is unknown. Hence the approach is to apply a repelling force if during trilinear velocity interpolation for a particle on the grid, at least one of the eight grid points is gas. The force is applied by replacing the unknown velocity of the gas point with the lattice speed of sound ( $\frac{1}{\sqrt{3}}$  grid cells per time step, the fastest velocity possible in LBM units) in direction

opposed to the local surface normal approximation. In case of a sticky surface, an attractive force is applied if at least one of the eight points is interface. This is done by adding the lattice speed of sound in the direction of the local surface normal approximation to the fluid velocity at the interface point.

In nature, other electrostatic interactions between particles bubble vortex also play a role [51], which are neglected by our simplified model. Further, the shear forces in the bubble vortex may separate particle aggregates and enhance particle fragmentation, but these effects are also not taken into account, as we only study non-interacting, single particles.

### Simulation parameters

All simulations are carried out with these parameters for water: kinematic shear viscosity  $\nu = 1.0 \cdot 10^{-6} \frac{\text{m}^2}{\text{s}}$ , density  $\rho = 1000 \frac{\text{kg}}{\text{m}^3}$ , surface tension  $\sigma = 0.072 \frac{\text{kg}}{\text{s}^2}$ , gravitational acceleration  $g = 9.81 \frac{\text{m}}{\text{s}^2}$ . To eliminate one possible complication in the model, the microplastic particles have neutral buoyancy with a density of  $\rho_p = 1000 \frac{\text{kg}}{\text{m}^3}$ .

With a resulting Bond number of  $Bo = 2.18$  and Morton number  $Mo = 2.63 \cdot 10^{-11}$ , the expected bubble behavior is between “spherical” and “wobbling” [52]. This behavior is matched by our simulations (Figs. 1 and 3).

### Results and discussion

Rising bubbles in a water column can pick up particles in a process known as bubble scavenging [8–12]. Other works have already found that the microplastic concentration at the water surface is enriched [39–41], yet the mechanism for this enrichment is not identified. This suggests that bubble scavenging may apply to microplastic particles as well. We quantify this on a model system with computer simulations.

It is expected that weathered particles in nature stick less to the water surface due to their increased hydrophilicity [7, 53–55]. Thus we separately investigate the transport of weathered, non-sticky particles, and clean, sticky particles.

The simulation box geometry is  $1.6 \text{ cm} \times 1.6 \text{ cm} \times 12.8 \text{ cm}$  (Figs. 1 and 3) and the boundaries in horizontal directions are periodic. One bubble with diameter  $d_b = 4 \text{ mm}$  is initially placed at  $z_{\text{initial}} = d_b$  and the simulation is terminated once the bubble reaches the position  $z_{\text{final}} = 32 d_b - d_b$ , so the bubble travels a total distance of  $h_b = 12 \text{ cm}$ . The microplastic particle concentration is set to  $C = 10^5$  particles per  $\text{cm}^3$ . The total particle count is about 3269298 with slight variation depending on lattice resolution in the simulation. A concentration this high allows to obtain accurate particle counts with just a single simulation. In simulation units, the bubble diameter is set to  $d_b^{\text{sim}} = 74$ . This corresponds to the

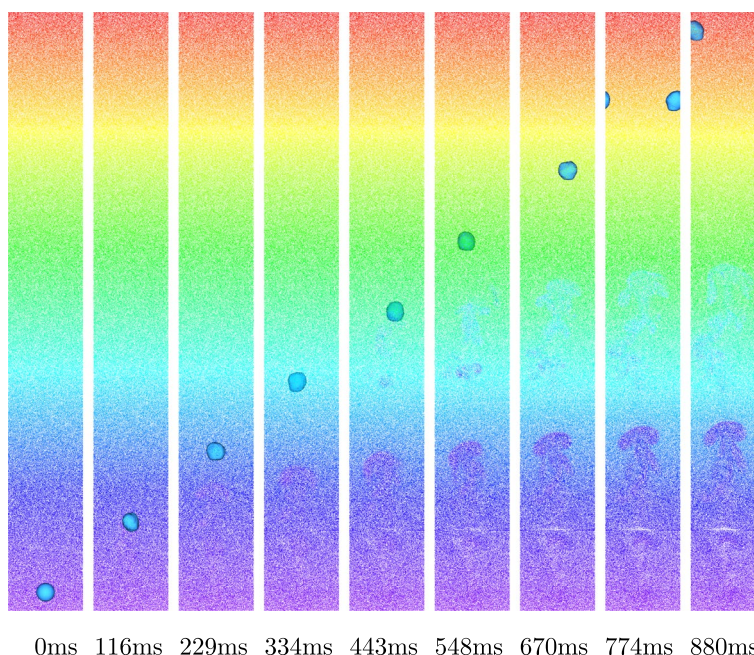


**Fig. 1** Illustration of the simulation for the rising bubble (particles do not stick to the bubble). The bubble ascends in a spiral as a result of non-laminar flow. Particles are colored by initial z-position. Images are not in uniform time intervals, but in uniform intervals of traveled distance. This figure is provided as a video in the [Supplementary file](#)

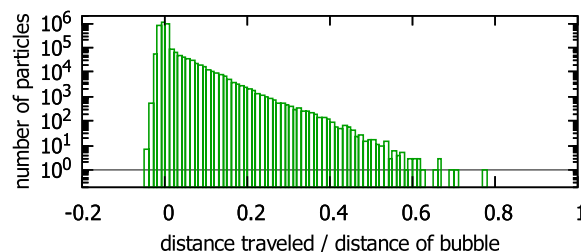
maximum box size allowed by the 40GB GPU memory on the Nvidia A100 which is used in the present simulations.

The simulated bubble travels the distance of  $h_b = 0.12$  m in  $t = 0.88$  s, resulting in an average velocity of  $136 \frac{\text{mm}}{\text{s}}$  (equivalent to Reynolds number  $Re = 545$ ), less than the experimental value of approximately  $200 \frac{\text{mm}}{\text{s}}$  [56]. This is expected, because in the simulation, the bubble starts with zero velocity and the flow needs to accelerate first. The behavior of a mostly spherical, wobbling bubble matches experimental findings [52].

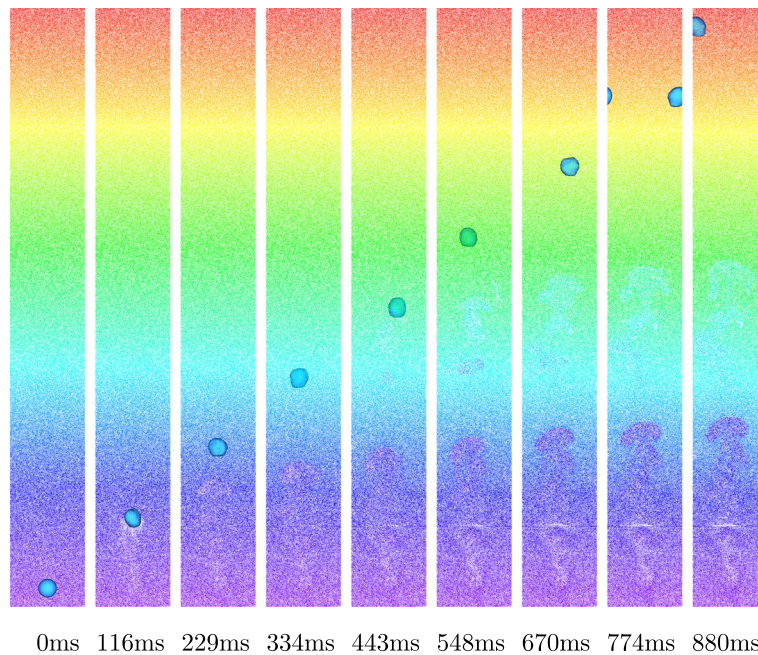
**Transport of non-sticky particles**

Figure 1 shows the simulation of the rising bubble where particles do not stick to the water surface. At first the bubble rises straight, but after the initial acceleration phase it pursues a spiraling trajectory, visible when it goes behind the slice of visualized particles and then comes back to front. This rotational behavior is consistent with experimental observations [51, 57]. At the end of the image series, the bubble passes half-way through the lateral periodic boundaries. Particles are colored by their initial z-position to be able to see where particles move in the vertical direction. A plume of particles is clearly visible in the lower half of the column, where the bubble still has been traveling in the plane of visualized particles.

In perfectly laminar flow and in the absence of additional effects beyond hydrodynamics, net particle transport through entrainment – particles dragged up by the flow around the bubble – would be impossible due to symmetry of the flow. Only when leaving the laminar regime, this transport mode is possible. Observations indicate that hydrophobic particles then may drop into the sub-bubble vortex [57]. The 4 mm diameter bubble is well outside the laminar flow regime at  $Re = 545$ , reflected in the clearly asymmetric distribution of traveled vertical particle distance in Fig. 2.



**Fig. 2** The distribution of the vertical travel distance of microplastic particles relative to the travel distance of the bubble. In this simulation, particles do not stick to the bubble. The vast majority of values are around 0 (logarithmic scale), but the distribution clearly is asymmetric towards positive distances, indicating particle entrainment as a consequence of non-laminar flow



**Fig. 3** Illustration of the simulation for the rising bubble (particles stick to the bubble). Particles are colored by initial z-position. Images are not in uniform time intervals, but in uniform intervals of traveled distance. The rising bubble initially plunges a void in particle concentration that quickly disappears again due to mixing. This figure is provided as a video in the [Supplementary files](#)

When taking the average of the traveled vertical distance for all particles and dividing by the traveled vertical distance of the bubble,  $h_{avg,rel} = \frac{1}{h_b} \frac{1}{N} \sum_{i=1}^N h_i = -8.56 \cdot 10^{-4}$ , with  $N = 3269298$ , the value is negative. This is expected, because the bubble volume, devoid of particles, starts at the bottom and moves to the top, so the fluid containing the particles has a net downward movement. To compute the net particle movement, the number of particles expected in the bubble volume  $N_b = C \cdot \frac{\pi}{6} d_b^3 = 3351$ , times the distance traveled by the bubble  $h_b = 0.12$  m is added:

$$h_{avg,rel,net} = \frac{1}{h_b} \frac{1}{N + N_b} \left( N_b h_b + \sum_{i=1}^N h_i \right) = \tag{2}$$

$$= \frac{1}{h_b} \frac{1}{N + N_b} (N_b h_b + h_{avg,rel} N h_b) = \tag{3}$$

$$= \frac{1}{N + N_b} (N_b + h_{avg,rel} N) = \tag{4}$$

$$= +1.69 \cdot 10^{-4} \tag{5}$$

So overall the net movement almost cancels out.

**Transport of sticky particles**

A possibly very efficient mechanism for particle transport is sticking of particles to the water-air interface of

the bubble thus dragging the particles along with the rising bubble as shown in Fig. 3. Indeed, in simulations with sticking particles, the distribution of traveled vertical distance in Fig. 4 shows that the bubble picks up more and more particles along its ascent and transports them the remaining way up.

The average relative particle distance  $h_{avg,rel} = \frac{1}{h_b} \frac{1}{N} \sum_{i=1}^N h_i = +2.84 \cdot 10^{-3}$  now is clearly positive. The net average relative particle distance

$$h_{avg,rel,net} = +3.86 \cdot 10^{-3} \tag{6}$$

then also is positive, meaning direct capture does enrich the particle concentration at the water surface.

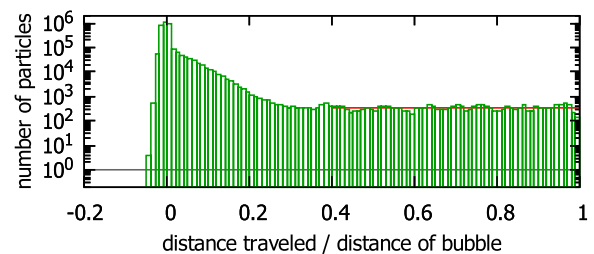


**Fig. 4** The distribution of the vertical travel distance of microplastic particles relative to the travel distance of the bubble. Here particles stick to the bubble. The bubble picks up new particles along the entire distance of travel and transports them to the top, visible as a plateauing distribution highlighted by the red line

Figure 4 shows the effects of both particle entrainment and direct capture. A plateau is visible from about  $0.4 h_b$  to  $1.0 h_b$  (red line). From this plateau we calculate an effective cross-section area in which any particle gets stuck to the ascending bubble: While the bubble travels between  $0.4 h_b$  to  $1.0 h_b$ , traversing a distance of  $h = 0.072$  m, it picks up  $N = 20369$  particles. With the known initial concentration of  $C = 10^5$  particles per  $\text{cm}^3$ , this number of particles corresponds to a fluid volume of  $V = \frac{N}{C} = 2.0 \cdot 10^{-7} \text{ m}^3$  and cylindrical cross-section area  $A = \frac{V}{h} = 2.83 \cdot 10^{-6} \text{ m}^2$ . This is  $\frac{A}{(d_b/2)^2 \pi} = 23\%$  of the cross-section area of the bubble, along which the bubble picks up any particle that it encounters and transports it to the surface. In other words, particles in the inner part of the cylindrical column of water above the bubble, when following the streamlines in the flow field created by the bubble, get close enough to the water surface on the upper half of the bubble to stick to it.

Finally, we verify the influence of numerical grid resolution on our results. For lower simulation resolution, we find cross-section areas of 29% ( $d_b^{\text{sim}} = 48$ ), 31% ( $d_b^{\text{sim}} = 32$ ) and 38% ( $d_b^{\text{sim}} = 24$ ), all of which are similar to 23% in Fig. 4. The larger values for lower resolution are a result of the hard-potential around the bubble surface extending by one lattice point, so for a smaller bubble in simulation units, the relative thickness of the hard potential is larger, increasing the bubble radius of influence where particles adhere to the interface.

## Conclusions

On the simulation model of a 4 mm diameter air bubble, we investigated the interactions between microplastic particles and air bubbles in water during bubble scavenging, when particle diameters are significantly smaller than the bubble diameter. We considered two possible mechanisms: entrainment – particles being dragged up in the non-laminar flow caused by the bubble – and direct capture – particles sticking to the bubble. The sticking mechanism is expected to be particularly relevant for hydrophobic microplastic particles. Pristine particles are indeed rather hydrophobic and thus tend to stick to bubbles, but become increasingly hydrophilic when left weathering in the environment, sticking less to bubbles. Our simulations indicate that the direct capture mechanism significantly increases vertical upward transport in the water column when bubbles are present. We therefore conclude that particle weathering may decrease upward transport in the water column during bubble scavenging. However, future laboratory experiments are needed to confirm our results.

## Abbreviations

LBM Lattice Boltzmann method

VoF Volume-of-Fluid  
IBM Immersed-boundary method  
SML Sea surface microlayer

## Supplementary Information

The online version contains supplementary material available at <https://doi.org/10.1186/s43591-023-00053-7>.

**Additional file 1.** Figures 1 and 3 as video files.

## Acknowledgements

We acknowledge the NVIDIA Corporation for donating a Titan Xp GPU and an A100 40GB GPU for our research.

## Authors' contributions

ML and FH implemented and validated the simulation software. ML conducted the simulations and evaluated the data. ML and SG contributed to study design. ML wrote the manuscript. The authors read and approved the final manuscript.

## Funding

Open Access funding enabled and organized by Projekt DEAL. This study was funded by the Deutsche Forschungsgemeinschaft (DFG, German Research Foundation) - SFB 1357 - 391977956, and Number 491183248. Funded by the Open Access Publishing Fund of the University of Bayreuth.

## Availability of data and materials

The data sets used and/or analyzed during the current study are publicly available on Zenodo and the simulation source code is available from the corresponding author upon reasonable request.

## Declarations

### Ethics approval and consent to participate

Not applicable.

### Consent for publication

Not applicable.

### Competing interests

The authors declare no competing interests.

Received: 19 October 2022 Accepted: 31 January 2023

Published online: 11 February 2023

## References

- Koga M. Bubble entrainment in breaking wind waves. *Tellus*. 1982;34(5):481–9.
- Weber ME, Blanchard DC, Syzdek LD. The mechanism of scavenging of waterborne bacteria by a rising bubble. *Limnol Oceanogr*. 1983;28(1):101–5.
- Mileva E. Solid particle in the boundary layer of a rising bubble. *Colloid Polym Sci*. 1990;268(4):375–83.
- Nguyen AV, Ralston J, Schulze HJ. On modelling of bubble-particle attachment probability in flotation. *Int J Miner Process*. 1998;53(4):225–49.
- Phan CM, Nguyen AV, Miller JD, Evans GM, Jameson GJ. Investigations of bubble-particle interactions. *Int J Miner Process*. 2003;72(1–4):239–54.
- Xing Y, Gui X, Pan L, Pinchasik BE, Cao Y, Liu J, et al. Recent experimental advances for understanding bubble-particle attachment in flotation. *Adv Colloid Interf Sci*. 2017;246:105–32.
- Ahmadi P, Elagami H, Dichgans F, Schmidt C, Gilfedder B, Frei S, et al. Systematic evaluation of physical parameters affecting the terminal settling velocity of microplastic particles in lakes using cfd. *front. Environ Sci*. 2022;10:875220.

8. Carlucci A, Williams P. Concentration of bacteria from sea water by bubble scavenging. *ICES J Mar Sci.* 1965;30(1):28–33.
9. Blanchard DC, Syzdek LD, Weber ME. Bubble scavenging of bacteria in freshwater quickly produces bacterial enrichment in airborne jet drops. *Limnol Oceanogr.* 1981;26(5):961–4.
10. Aller JY, Kuznetsova MR, Jahns CJ, Kemp PF. The sea surface microlayer as a source of viral and bacterial enrichment in marine aerosols. *J Aerosol Sci.* 2005;36(5–6):801–12.
11. Walls PL, Bird JC. Enriching particles on a bubble through drainage: measuring and modeling the concentration of microbial particles in a bubble film at rupture. *Elementa Sci Anthropocene.* 2017;5:34.
12. Marks R, Górecka E, McCartney K, Borkowski W. Rising bubbles as mechanism for scavenging and aerosolization of diatoms. *J Aerosol Sci.* 2019;128:79–88.
13. Spiel DE. The sizes of the jet drops produced by air bubbles bursting on sea-and fresh-water surfaces. *Tellus B Chem Phys Meteorol.* 1994;46(4):325–38.
14. Wu J. Jet drops produced by bubbles bursting at the surface of seawater. *J Phys Oceanogr.* 2002;32(11):3286–90.
15. Walls PL, Henaux L, Bird JC. Jet drops from bursting bubbles: How gravity and viscosity couple to inhibit droplet production. *Phys Rev E.* 2015;92(2):021002.
16. Ghabache E, Séon T. Size of the top jet drop produced by bubble bursting. *Phys Rev Fluids.* 2016;1(5):051901.
17. Walls PL, McRae O, Natarajan V, Johnson C, Antoniou C, Bird JC. Quantifying the potential for bursting bubbles to damage suspended cells. *Sci Rep.* 2017;7(1):1–9.
18. Deike L, Ghabache E, Liger-Belair G, Das AK, Zaleski S, Popinet S, et al. Dynamics of jets produced by bursting bubbles. *Phys Rev Fluids.* 2018;3(1):013603.
19. Berry A, Deike L, Séon T, Popinet S. Role of all jet drops in mass transfer from bursting bubbles. *Phys Rev Fluids.* 2020;5(3):033605.
20. Berry A, Popinet S, Séon T, Deike L. Statistics of jet drop production. *Geophys Res Lett.* 2021;48(10):e2021GL092919.
21. Blanco-Rodríguez FJ, Gordillo J. On the jets produced by drops impacting a deep liquid pool and by bursting bubbles. *J Fluid Mech.* 2021;916:A37.
22. Woodcock A. Bursting bubbles and air pollution. *Sew Ind Wastes.* 1955;27(10):1189–92.
23. Afeti G, Resch F. Distribution of the liquid aerosol produced from bursting bubbles in sea and distilled water. *Tellus B.* 1990;42(4):378–84.
24. Lhuissier H, Villermaux E. Bursting bubble aerosols. *J Fluid Mech.* 2012;696:5–44.
25. Ji B, Yang Z, Feng J. Compound jetting from bubble bursting at an air-oil-water interface. *Nat Commun.* 2021;12(1):1–10.
26. Blanchard DC, Syzdek LD. Water-to-air transfer and enrichment of bacteria in drops from bursting bubbles. *Appl Environ Microbiol.* 1982;43(5):1001–5.
27. Blanchard DC. The ejection of drops from the sea and their enrichment with bacteria and other materials: a review. *Estuaries.* 1989;12(3):127–37.
28. Tseng RS, Viechnicki JT, Skop RA, Brown JW. Sea-to-air transfer of surface-active organic compounds by bursting bubbles. *J Geophys Res Oceans.* 1992;97(C4):5201–6.
29. Masry M, Rossignol S, Roussel BT, Bourgogne D, Bussièrè PO, R'mili B, et al. Experimental evidence of plastic particles transfer at the water-air interface through bubble bursting. *Environ Pollut.* 2021;280:116949.
30. Shiu RF, Chen LY, Lee HJ, Gong GC, Lee C. New insights into the role of marine plastic-gels in microplastic transfer from water to the atmosphere via bubble bursting. *Water Res.* 2022;222:118856.
31. Ji B, Singh A, Feng J. Water-to-Air Transfer of Nano/Microsized Particulates: Enrichment Effect in Bubble Bursting Jet Drops. *Nano Lett.* 2022.
32. Yang S, Zhang T, Gan Y, Lu X, Chen H, Chen J, et al. Constraining microplastic particle emission flux from the ocean. *Environ Sci Technol Lett.* 2022;9(6):513–9.
33. Dubitsky L, McRae O, Bird JC. Enrichment of scavenged particles in jet drops determined by bubble size and particle position. *Phys Rev Lett.* 2023;130(5):054001.
34. Lehmann M, Oehlschlägel LM, Häußl FP, Held A, Gekle S. Ejection of marine microplastics by raindrops: a computational and experimental study. *Microplastics Nanoplastics.* 2021;1(18):1–19.
35. Pabortsava K, Lampitt RS. High concentrations of plastic hidden beneath the surface of the Atlantic Ocean. *Nat Commun.* 2020;11(1):1–11.
36. ALdF Lacerda, LdS Rodrigues, E Van Sebbile, FL Rodrigues, L Ribeiro, ER Secchi, et al. Plastics in sea surface waters around the Antarctic Peninsula. *Sci Rep.* 2019;9(1):1–12.
37. Naidoo T, Glassom D. Sea-surface microplastic concentrations along the coastal shelf of KwaZulu-Natal. *South Africa Mar Pollut Bull.* 2019;149:110514.
38. Gajšt T, Bizjak T, Palatinus A, Liubartseva S, Kržan A. Sea surface microplastics in Slovenian part of the Northern Adriatic. *Mar Pollut Bull.* 2016;113(1–2):392–9.
39. Song YK, Hong SH, Jang M, Kang JH, Kwon OY, Han GM, et al. Large accumulation of micro-sized synthetic polymer particles in the sea surface microlayer. *Environ Sci Technol.* 2014;48(16):9014–21.
40. Chae DH, Kim IS, Kim SK, Song YK, Shim WJ. Abundance and distribution characteristics of microplastics in surface seawaters of the Incheon/Kyeonggi coastal region. *Arch Environ Contam Toxicol.* 2015;69(3):269–78.
41. Anderson ZT, Cundy AB, Croudace IW, Warwick PE, Celis-Hernandez O, Stead JL. A rapid method for assessing the accumulation of microplastics in the sea surface microlayer (SML) of estuarine systems. *Sci Rep.* 2018;8(1):1–11.
42. Laermans H, Lehmann M, Klee M, Löder MG, Gekle S, Bogner C. Tracing the horizontal transport of microplastics on rough surfaces. *Nanoplastics.* 2021;1(11):1–12.
43. Häußl F. MPI-based multi-GPU extension of the Lattice Boltzmann Method. 2019. <https://epub.uni-bayreuth.de/5689/>. Accessed 30 June 2021.
44. Lehmann M. High performance free surface LBM on GPUs. 2019. <https://epub.uni-bayreuth.de/5400/>. Accessed 02 June 2021.
45. Lehmann M, Krause MJ, Amati G, Segal M, Harting J, Gekle S. Accuracy and performance of the lattice Boltzmann method with 64-bit, 32-bit, and customized 16-bit number formats. *Phys Rev E.* 2022;106:015308. <https://doi.org/10.1103/PhysRevE.106.015308>.
46. Lehmann M, Gekle S. Analytic Solution to the Piecewise Linear Interface Construction Problem and Its Application in Curvature Calculation for Volume-of-Fluid Simulation Codes. *Computation.* 2022;10(2):21.
47. Häußl F. Soft Objects in Newtonian and Non-Newtonian Fluids: a Computational Study of Bubbles and Capsules in Flow. 2022. <https://epub.uni-bayreuth.de/5960/>.
48. Frijters S, Krüger T, Harting J. Parallelised Hoshen-Kopelman algorithm for lattice-Boltzmann simulations. *Comput Phys Commun.* 2015;189:92–8.
49. Schwarzmeier C, Holzer M, Mitchell T, Lehmann M, Häußl F, Rüdè U. Comparison of free surface and conservative Allen-Cahn phase field lattice Boltzmann method. 2022. arXiv preprint [arXiv:2206.11637](https://arxiv.org/abs/2206.11637).
50. Choy CA, Robison BH, Gagne TO, Erwin B, Firl E, Halden RU, et al. The vertical distribution and biological transport of marine microplastics across the epipelagic and mesopelagic water column. *Sci Rep.* 2019;9(1):1–9.
51. Marks R. Bubble mediated polymerization of RNA and DNA. *AIMS Biophys.* 2022;9(2):96–107.
52. Clift R, Grace JR, Weber ME. Bubbles, drops, and particles. New York: Dover Publications Inc.; 2005.
53. Al Harraq A, Bharti B. Microplastics through the Lens of Colloid Science. *ACS Environ Au.* 2021;2(1):3–10.
54. Changfu Y, Jiani G, Yidi Y, Yijin L, Yiyao L, Yu F. Interface behavior changes of weathered polystyrene with ciprofloxacin in seawater environment. *Environ Res.* 2022;212:113132.
55. Liu G, Zhu Z, Yang Y, Sun Y, Yu F, Ma J. Sorption behavior and mechanism of hydrophilic organic chemicals to virgin and aged microplastics in freshwater and seawater. *Environ Pollut.* 2019;246:26–33.
56. Kugou N, Ishida K, Yoshida A. Experimental study on motion of air bubbles in seawater (terminal velocity and drag coefficient of air bubble rising in seawater). *WIT Trans Built Environ.* 2003;68:145–58.
57. Marks R. Bubble rotational features-preliminary investigations. *Oceanogr Open Access.* 2014;2(4):1–6.

## Publisher's Note

Springer Nature remains neutral with regard to jurisdictional claims in published maps and institutional affiliations.